



Article

Classification of Garlic (*Allium sativum* L.) Crops by Fertilizer Differences Using Ground-Based Hyperspectral Imaging System

Hwanjo Chung ¹, Seunghwan Wi ², Byoung-Kwan Cho ³  and Hoonsoo Lee ^{1,*} 

¹ Department of Biosystems Engineering, College of Agriculture, Life & Environment Science, Chungbuk National University, 1 Chungdae-ro, Seowon-gu, Cheongju-si 28644, Republic of Korea

² Vegetable Research Division, National Institute of Horticultural & Herbal Science, Wanju 55365, Republic of Korea; kgad@korea.kr

³ Department of Biosystems Machinery Engineering, College of Agricultural and Life Science, Chungnam National University, 99 Daehak-ro, Yuseoung-gu, Daejeon 34134, Republic of Korea

* Correspondence: hslee202@cbnu.ac.kr

Abstract: In contemporary agriculture, enhancing the efficient production of crops and optimizing resource utilization have become paramount objectives. Garlic growth and quality are influenced by various factors, with fertilizers playing a pivotal role in shaping both aspects. This study aimed to develop classification models for distinguishing garlic fertilizer application differences by employing statistical and machine learning techniques, such as partial least squares (PLS), based on data acquired from a ground-based hyperspectral imaging system in the agricultural sector. The garlic variety chosen for this study was Hongsan, and the fertilizer application plots were segmented into three distinct sections. Data were acquired within the VIS/NIR wavelength range using hyperspectral imaging. Following data acquisition, the standard normal variate (SNV) pre-processing technique was applied to enhance the dataset. To identify the optimal wavelengths, various techniques such as sequential forward selection (SFS), successive projections algorithm (SPA), variable importance in projection (VIP), and interval partial least squares (iPLS) were employed, resulting in the selection of 12 optimal wavelengths. For the fertilizer application difference model, six integrated vegetation indices were chosen for comparison with existing growth indicators. Using the same methodology, the model construction showed accuracies of 90.7% for PLS. Thus, the proposed model suggests that efficient regulation of garlic fertilizer application can be achieved by utilizing statistical and machine learning techniques.

Keywords: hyperspectral imaging; machine learning; ground-based hyperspectral imaging system; garlic; fertilizer



Citation: Chung, H.; Wi, S.; Cho, B.-K.; Lee, H. Classification of Garlic (*Allium sativum* L.) Crops by Fertilizer Differences Using Ground-Based Hyperspectral Imaging System. *Agriculture* **2024**, *14*, 1215. <https://doi.org/10.3390/agriculture14081215>

Academic Editor: Hongbin Pu

Received: 1 July 2024

Revised: 18 July 2024

Accepted: 22 July 2024

Published: 24 July 2024



Copyright: © 2024 by the authors. Licensee MDPI, Basel, Switzerland. This article is an open access article distributed under the terms and conditions of the Creative Commons Attribution (CC BY) license (<https://creativecommons.org/licenses/by/4.0/>).

1. Introduction

Garlic (*Allium sativum* L.) is an ancient plant that has a significant impact on various cultures and culinary traditions. In civilizations such as Greece, Rome, China, and India, garlic has been widely utilized as a medicinal herb, seasoning, and spice [1]. Garlic is widely used and extensively employed in various cuisines. It comes in numerous varieties and is primarily produced in countries such as China, India, Russia, and South Korea. Garlic, cherished by many for its distinctive aroma and flavor, not only appeals to people's taste buds but also exerts positive effects on health. It offers various health benefits, such as antimicrobial and anti-inflammatory properties and regulation of blood pressure and cholesterol, contributing positively to overall well-being [2]. The International Trade Centre (ITC) trade map data indicate that the global garlic market recorded an import value of USD 7.3 billion in 2021, showing growth. Subsequently, in 2022, the import value increased further to USD 7.5 billion. Garlic has established itself as a plant that goes beyond being a simple food ingredient and plays a significant role in positively affecting both health and the economy.

Several factors influence the growth and quality of garlic; however, two key factors are environmental and fertilizer conditions. Among these, fertilizers are crucial because they need to be applied early in the growth period to ensure that the plant receives the necessary nutrients throughout its growth stage. The type and quantity of fertilizer used can also affect garlic growth. Proper fertilization can rapidly increase nutrient levels; however, insufficient fertilization can hinder crop growth, and excessive fertilization can have adverse effects on the soil, crop productivity, and the environment [3]. Therefore, judicious fertilizer use is essential for the cultivation of healthy and high-yielding garlic crops. Conventional research has actively utilized growth indicators like the NDVI to assess the conditions of such crops [4]. The NDVI value is closely related to crop density; however, accurately assessing crop growth status becomes challenging when the value falls outside a particular range. In addition, it can vary depending on the crop type, and using a generalized value for all crops may result in reduced accuracy [5]. Therefore, recent research has actively utilized hyperspectral imaging to nondestructively analyze the crop growth status for more accurate acquisition and analysis of growth information [6]. Hyperspectral imaging combines spectral technology with spatial data, captures 2D image information based on the spectral bands of electromagnetic waves, and organizes them into a 3D cube. This technology provides valuable information on the physiological and biochemical states of crops, such as their moisture content, nutrient absorption, and responses to diseases or stress [7].

An RGB image typically consists of three primary colors: red, green, and blue, each represented by specific wavelengths. For RGB, red is approximately 620–750 nm, green is approximately 495–570 nm, and blue is approximately 450–495 nm. By contrast, hyperspectral images capture a much broader range of wavelengths, typically in the range of 10–100 spectral bands. Notably, different studies or applications may focus on specific spectral bands within the VIS and NIR ranges based on their research objectives or the particular needs of the agricultural task at hand, as mentioned in Ravikanth, Jayas [8]. A hyperspectral imaging system is composed of various components, including a light source, an optical system, a spectral dispersion device, and an image sensor. In the line-scan hyperspectral imaging method, the system simultaneously captures the overall spectral information for each spatial point within the linear field of view (FOV) while also obtaining spatial information through a slit. This method results in the generation of a particular 2D image represented by coordinates (y, λ) , where “ y ” denotes one spatial dimension, and “ λ ” represents one spectral dimension. Each scan contributes to the construction of a complete hyperspectral cube (x, y, λ) , where “ x ” is the moving direction along which the scan is performed. This process continues until the entire surface of the sample is covered. Hyperspectral imaging technology has been employed in several agricultural studies. This technology enables researchers and practitioners to gather detailed information on the spectral characteristics of agricultural samples [9]. By analyzing hyperspectral data, valuable insights can be gained into various aspects of crop health, nutrient levels, stress conditions, and other parameters that affect plant growth. The ability to capture both spatial and spectral information simultaneously makes hyperspectral imaging a powerful tool for precision agriculture and crop monitoring. Researchers can use these data to develop models and algorithms for crop classification, disease detection, and yield prediction, contributing to more efficient and informed agricultural practices.

Tao, Feng [10] estimated the yield and plant height of winter wheat using hyperspectral images. Baek, Lee [11] generated a regression model of total volatile basic nitrogen (TVB-N) content in fresh pork using spectral SWIR images. Geipel, Bakken [12] conducted forage yield and quality assessments through UAV and hyperspectral imaging. Gui, Fei [13] detected soybean mosaic virus disease (SMV) in soybeans based on hyperspectral imaging techniques. Sabzi, Pourdarbani [14] classified cucumber leaves according to their nitrogen content using hyperspectral imaging to identify excess nitrogen. Chu, Miao [15] performed green banana maturity classification and quality evaluation using hyperspectral imaging. Kim, Lee [16] developed a short-wave infrared (SWIR) HSI system for the rapid detection

of benzoyl peroxide (BPO) particles in flour. In agriculture, hyperspectral image data are primarily acquired using satellites or aircraft [17]. While the use of satellites and aircraft provides the advantage of covering large areas in a short time, the associated high cost and susceptibility to atmospheric conditions, such as scattering, absorption, and reflection, can lead to distorted spectral characteristics and lower data quality [18].

In this study, we aimed to address the limitations of traditional vegetation indices (such as NDVI), which fail to capture subtle differences in fertilization levels, and the issues of atmospheric conditions and reduced image resolution faced by aerial and satellite-based hyperspectral imaging. To overcome these challenges, we utilized a ground-based hyperspectral imaging system to enhance resolution and reduce the impact of atmospheric conditions, with the objective of developing an optimal model for precision variable-rate fertilization of garlic crops. Specifically, we developed and compared models based on six growth indices, models using selected optimal wavelengths, and models using full wavelength data with machine learning techniques such as partial least squares (PLS). Additionally, we applied these models to hyperspectral images to visualize the effects of fertilization on garlic crops grown in the field.

2. Materials and Methods

2.1. Experimental Fields

The experiment was conducted in a test field at the Goheung Agricultural Technology Center, located at 143 Pungnam-ro, Pungyang-myeon, Goheung-gun, Jeollanam-do. The measurement area was 840 m², with a ground cover treatment using black vinyl. The growth map is shown in Figure 1. The standard composition of the fertilizers is detailed in Table 1. The organic fertilizer has a nitrogen (N), phosphorus (P), and potassium (K) ratio of 1:2:2, with a total amount of 2000 kg/10a. This includes 100 kg of nitrogen (N), 200 kg of phosphorus (P), and 200 kg of potassium (K). The remaining 1500 kg consists of organic matter, trace elements, moisture content, and other nutrients. The nitrogen levels were varied to create different treatment plots. Fertilization treatments were divided into three plots: non-treatment, standard fertilizer, and double fertilizer. Each plot received 0 kg/10a, 100 kg/10a, and 200 kg/10a of nitrogen, respectively. Garlic crops of the southern type were selected, with the chosen variety being Hongsan. The planting date was 29 August 2022, and the data were acquired in two sessions. The session during which garlic absorbs nutrients begins after the roots descend following planting. Initially, it relied primarily on the nutrients stored in garlic seeds. However, as growth progressed after winter and into spring, the absorption rate increased. According to garlic cultivation guidelines [19], active nutrient absorption continues until the bulb becomes enlarged, at which point leaf growth stops and nutrient absorption ceases. Therefore, data acquisition was conducted in April before the bulb enlargement phase and in May after its completion. In addition, to obtain yield data, the total fresh weight and bulb fresh weight of garlic crops was collected on the day of imaging.

Table 1. Composition of fertilizer fertilization of garlic crops.

Fertilizer	Total (kg/10a)	Basal Application of Fertilizer (kg/10a)	Additional Fertilizer (kg/10a)	
			First	Second
Organic fertilizer (N P K included)	2000	2000	-	-
Urea	54	20	17	17
Superphosphate	39	39	-	-
Potassium sulfate	40	14	13	13
Calcium	200	200	-	-

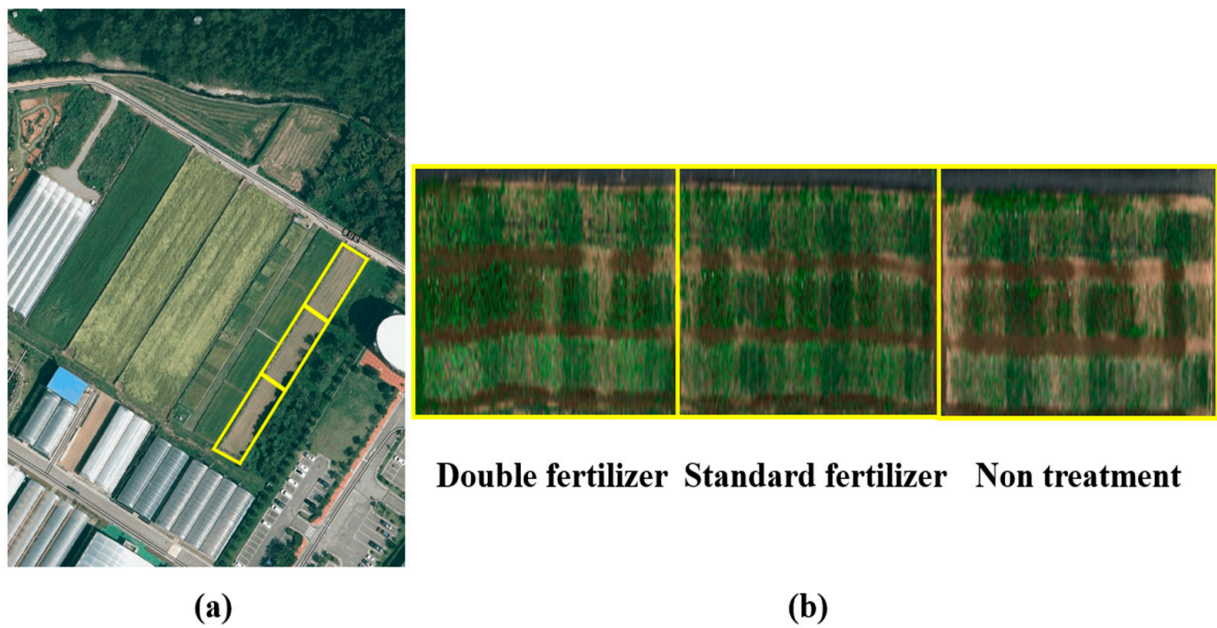


Figure 1. The study area for this research. (a) The garlic field located in Goheung-gun. (b) Three type of different fertilizer sector.

2.2. Construction of a Hyperspectral Imaging Ground Driving Platform

To address data loss and resolution degradation encountered in the acquisition of satellite and aerial hyperspectral image data, a ground-based hyperspectral imaging system module was developed, and research was conducted. Several factors must be considered for stable operation in a field environment. For field crops, slip may occur with conventional tires because of the high soil moisture content in the furrows after rainfall. Therefore, agricultural tires were selected, and considering the furrow width, 12-inch managerial tires were selected. To ensure stable driving control, a motor controller capable of on/off, direction change, and rotational speed adjustment for a 24 V, 300 W DC motor was developed. Rotation of the driving platform was achieved by controlling the four motors individually, allowing direction changes and forward/backward movements. The selection of driving motors should consider the overall weight of the driving platform and driving speed. Assuming a maximum weight of 150 kg for the driving platform and a selectable speed range of 2 km/h to 6 km/h, a minimum output of 1 kW was deemed necessary for the driving motor. Therefore, four 24 V, 300 W DC motors were used. The driving speed was controlled using a 1:100 reduction gear, considering the tire size and motor RPM. The driving power and image acquisition of the driving platform were supplied using a battery. The estimated power consumption was 1.2 kW for the driving motor, 500 W for the small barebone PC, and 100 W for the monitor. An inverter (24 V–220 V) was installed to supply power at 220 V to the monitor and the PC. Therefore, the total expected power consumption, considering the inverter efficiency, was estimated to be 2 kW. Because the driving motor operates at 24 V, a 24 V lithium-ion battery was used, and a 40 Ah capacity battery was installed, considering a 2 h acquisition time in one field. The completed driving module is illustrated in Figure 2.

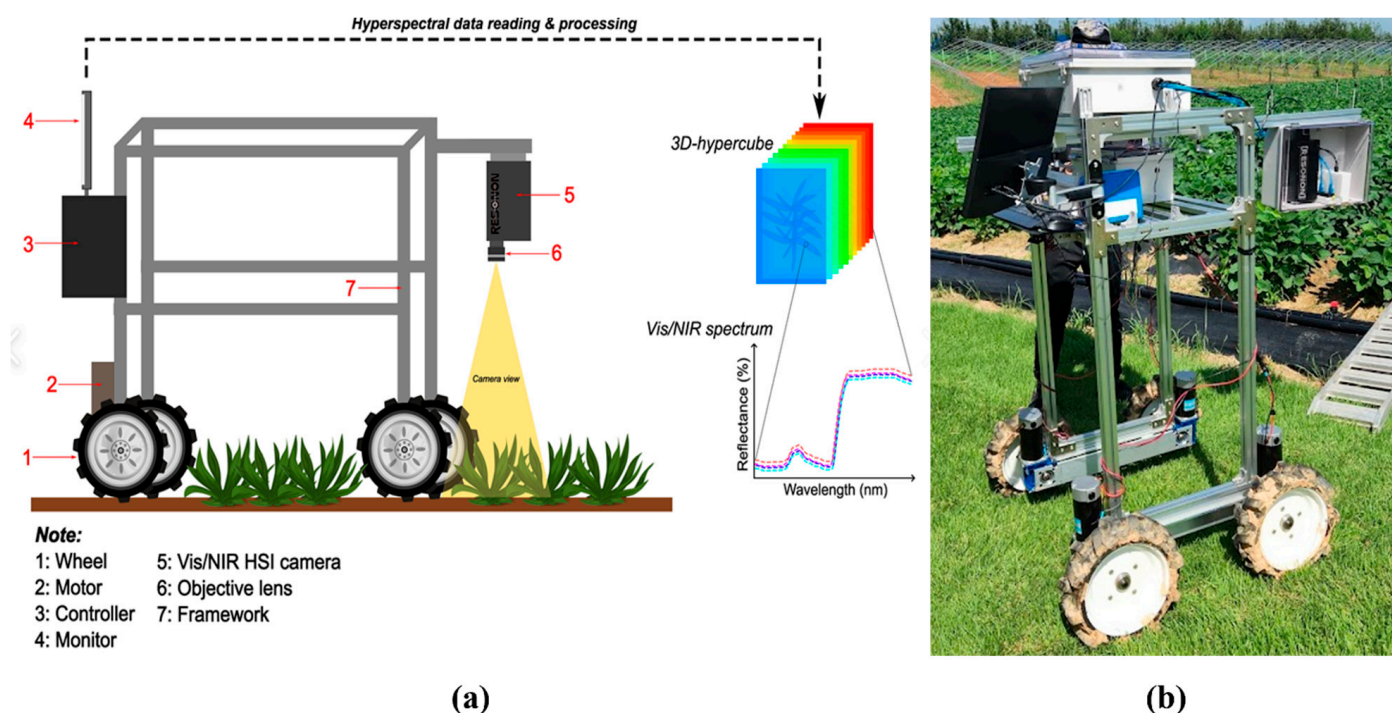


Figure 2. Ground-based hyperspectral imaging system module. (a) Component of module. (b) Actual manufactured hyperspectral imaging system module.

2.3. Image Acquisition and Calibration

In this study, for the development of an optimal model to predict the amount of fertilizer applied, a ground-based hyperspectral imaging system module was implemented, capable of assessing the growth status of field-cultivated garlic. The ground-based hyperspectral imaging system module comprised a hyperspectral camera and a stable field-driving module. The selection of the hyperspectral camera for this experiment considered the measurement wavelength range, wavelength resolution, spatial resolution, and frame rate (FPS). The Pika Xc2 model (Resonon Inc., Bozeman, MT, USA) was selected for this study. The specifications for the camera are shown in Table 2.

Table 2. Specifications of hyperspectral imaging camera.

Specifications	
Spectral Range	400–1000
Spectral Channels	447
Spectral Sampling (nm)	1.3
Spectral Resolution–FWHM (nm)	1.9
Spatial Pixels	1600
Frame Rate Second (FPS)	165
f/#	2.4
Dimensions (mm)	265 × 106 × 75

Before acquiring the hyperspectral image data, the original image must be corrected to black and white to reduce the influence of environmental factors. Therefore, the spectrum of the white-corrected image was obtained by capturing the hyperspectral image data of a white-balance target (Edmond Optics Inc., Barrington, NJ, USA) with a reflectance close to 100%. The spectrum of the black-corrected image was obtained by capturing a

hyperspectral image using a completely closed lens cap. After obtaining the two corrected spectra, the corrected image was calculated using the following formula:

$$D_n = \frac{D_r - D_b}{D_w - D_b} \times 100 \tag{1}$$

D_r represents the original images, D_w the white-calibration images, D_b the black-calibration images, and D_n the corrected images. The process of building the classification model after data acquisition is illustrated in Figure 3.

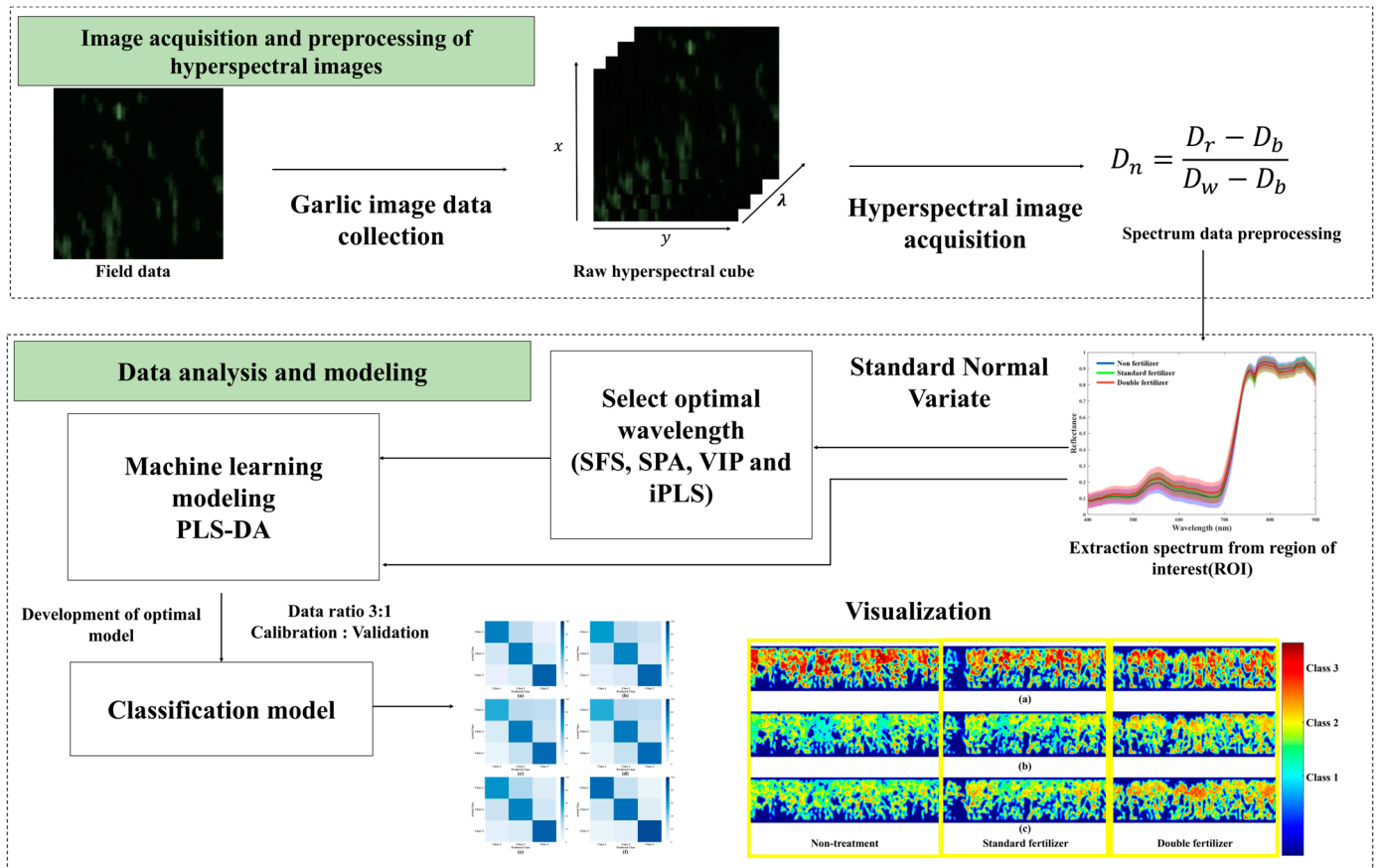


Figure 3. Process of building a hyperspectral image data classification model.

2.4. Region of Interest (ROI) Identification

Region of interest (ROI) selection was employed to isolate the garlic portion from the background in the hyperspectral images. The MATLAB 2022a software (MathWorks, Natick, MA, USA) was utilized for this purpose. The original hyperspectral image data are structured in three dimensions, comprising 3600 pixels in the x-direction, 107 pixels in the y-direction, and 187 bands in the z-direction, ranging from 403.3 nm to 898.5 nm. By applying a threshold to the grayscale image, a binary image was generated to remove background noise. Subsequently, the ROI was utilized to create a mask, facilitating the extraction of the garlic portion from the hyperspectral image data.

2.5. Vegetation Index

For comparison with the newly developed model, we developed the model using six well-known vegetation index values and investigated several key indices. The Normalized Difference Vegetation Index (NDVI) is a crucial ecological metric widely used in remote sensing and Earth observations. The NDVI is particularly valuable for evaluating plant growth and land cover conditions and is primarily extracted from satellite and aerial

imagery. The NDVI estimates the form and condition of vegetation by utilizing wavelengths in the red and NIR regions. This method provides an indirect means of assessing plant health, growth status, and soil moisture. The Photochemical Reflectance Index (PRI) utilizes the chlorophyll fluorescence response to gain insights into photosynthesis and its regulation. The PRI is primarily employed to detect and monitor fine-tuned adjustments related to the photosynthetic activity of plants. It is susceptible to wavelength absorption by chromophore pigments because of the photosynthetic fluorescence response at the picosecond scale [20]. Thus, the PRI can be helpful in detecting and understanding changes in photosynthetic activity. The Green Normalized Difference Vegetation Index (GNDVI) utilizes the reflectance in the NIR and green spectral bands for plant growth and vegetation index measurements. The GNDVI is a variant of the NDVI that is particularly useful for assessing the health and growth status of plants. It primarily uses the reflectance in the green spectral band to detect biological activity and green vegetation. This design makes the GNDVI exceptionally responsive when green color is abundant in the vegetation [21]. The RDVI (Renormalized Difference Vegetation Index) is an indicator used in the fields of ecology and agriculture to measure plant growth and health status. The RDVI is a variant of the NDVI that is designed to be more universally applicable in various environments by adjusting the range of the NDVI more appropriately [22]. The CI (Chlorophyll Index) is an indicator that provides information related to chlorophyll content. There are various CIs, and it is a simple yet effective chlorophyll content index that uses green and red wavelengths [23]. The Transformed Chlorophyll Absorption in Reflectance Index (TCARI) is a vegetation index based on the absorption characteristics of chlorophyll in plants. The TCARI is used to estimate the amount and activity of chlorophyll in plants by emphasizing the absorption band of chlorophyll-a [24]. The formulas for each vegetation index are listed in Table 3.

Table 3. Definitions of the vegetation indices.

Description	Index	Formula	Reference
Normalized Difference Vegetation Index	NDVI	$\frac{NIR_{800} + RED_{670}}{NIR_{800} - RED_{670}}$	[25]
Photochemical Reflectance Index	PRI	$\frac{Green_{531} - Green_{550}}{Green_{531} + Green_{550}}$	[20]
Green Normalized Difference Vegetation Index	GNDVI	$\frac{NIR_{800} - Green_{550}}{NIR_{800} + Green_{550}}$	[26]
Renormalized Difference Vegetation Index	RDVI	$\frac{NIR_{800} - RED_{670}}{\sqrt{NIR_{800} + RED_{670}}}$	[27]
Chlorophyll Index	CI	$\frac{RED_{670}}{Green_{550}} - 1$	[28]
Transformed Chlorophyll Absorption in Reflectance Index	TCARI	$3 * \left[(RED_{700} - RED_{670}) - 0.2 * (RED_{700} - RED_{670}) * \left(\frac{RED_{700}}{RED_{670}} \right) \right]$	[29]

2.6. Select Optimal Wavelength

In this study, the optimal wavelengths were selected to enhance the efficiency of the model performance and to choose wavelengths that effectively describe the variables. To achieve this, four methods were selected: sequential feature selection (SFS), successive projection algorithm (SPA), variable importance in projection (VIP), and interval partial least squares (iPLS). These advanced techniques, designed to address issues such as multicollinearity and high dimensionality, can be utilized to select optimal wavelengths for spectroscopic data [30]. SFS is a variable selection technique that involves iteratively adding or removing variables to determine the optimal set of variables. It starts with an empty set of variables and, at each step, selects or removes a variable to evaluate the performance of the model. This process helps to reduce model complexity and improves predictive performance [31]. The SPA is a method for both dimension reduction and variable selection. It aims to reduce the dimensions and select variables while retaining crucial information from the data. The SPA gradually reduces the feature space to identify significant variables, offering an effective approach for processing data by integrating variable selection and dimension reduction [32]. The VIP is a metric used to assess the importance of variables in multivariate data analysis. It is commonly employed in multivariate analysis techniques

such as PLS or PCA (principal component analysis). The VIP measures the impact of each variable on model prediction, aiding in the identification of essential variables. This ranks the importance of the variables, considering those with higher VIP scores as contributing more significantly to the model [33]. iPLS is a notable technique for multivariate data analysis and predictive modeling. This technology is particularly effective in handling multicollinearity issues. iPLS allows modeling by considering data segmentation and prediction uncertainty. It provides a variable selection feature through feature selection, allowing the construction of models by choosing only important variables instead of using all the independent variables. This helps make the model more concise, enhances the predictive performance, and allows the model to perform predictions for each interval through data segmentation. The predictions for each interval can be combined to obtain the result [34].

2.7. Modeling Methods

The preprocessing was applied using the standard normal variate (SNV) method. SNV effectively removes unwanted variations caused by factors such as light scattering and surface roughness, resulting in enhanced discrimination between different classes in the garlic crop data [35]. The analysis aimed to differentiate garlic crops based on different fertilization treatments: non-treatment (class 1), standard fertilization (class 2), and double fertilization (class 3). Partial least squares discriminant analysis (PLS-DA) is a statistical technique primarily used to emphasize the differences between classes in multivariate data and address classification problems. This proves to be particularly useful when there are numerous predictor variables or when there is multicollinearity among the predictor variables. PLS-DA projects predictor and response variables onto a new set of latent variables [36]. Therefore, this study employed this method to distinguish the differences caused by fertilizer application in garlic crops. PLS-DA is particularly effective at extracting meaningful features from high-dimensional spectral data and performing classification while reducing data dimensionality. Generally, in PLS, latent variables are chosen to maximize the covariance between the predictor and response variables. Subsequently, a regression analysis was performed on the response variables with latent variables to build the model [37]. The matrix calculation for the PLS-DA model concerning the latent variables can be expressed by Equation (2) below:

$$\begin{aligned} X &= TP^T + E \\ Y &= UQ^T + F \end{aligned} \quad (2)$$

X is a matrix of predictor variables, and Y is a matrix of response variables, where T and U represent the projections of X (X score, component, or factor matrix) and Y , respectively. P and Q are the loading matrices, and matrices E and F are the error terms, which are assumed to be independent and identically distributed random normal variables.

In this study, the LOOCV (leave-one-out cross-validation) method was applied to evaluate the performance of the PLS-DA model and to determine the number of variables. The ratio of the calibration to validation datasets in this approach was set at 3:1. Model performance was assessed using the coefficient of determination (R^2), with higher R^2 values indicating a better model.

Accuracy in classification measures how accurately a model predicts classes. It is calculated as the percentage of correctly classified samples out of all samples. Higher accuracy indicates better model performance. To measure accuracy, we used the following formula:

$$ACC(\%) = \frac{TP + TN}{TP + FP + TN + FN} \times 100 \quad (3)$$

where TP stands for true positives, TN for true negatives, FP for false positives, and FN for false negatives.

Thereafter, to visualize the classification of each class, an optimal model was constructed, and an image was generated using the obtained beta-coefficients.

Precision measures the proportion of true positive predictions out of the total positive predictions made by the model. It focuses on the accuracy of the positive class predictions. High precision indicates a low number of false positive errors. It is calculated as

$$Precision(\%) = \frac{TP}{TP + FP} \times 100 \quad (4)$$

Recall measures the proportion of true positive predictions out of the actual positive cases. It focuses on the model's ability to correctly identify all positive instances. High recall indicates a low number of false negative errors. It is calculated as

$$Recall(\%) = \frac{TP}{TP + FN} \times 100 \quad (5)$$

The F1 score is the harmonic mean of precision and recall, providing a balance between the two metrics. It is particularly useful when the class distribution is imbalanced, ensuring that both false positives and false negatives are considered. The F1 score helps provide a more comprehensive evaluation of the model's performance, especially in cases where the dataset might have imbalanced classes. It is calculated as

$$F1\ Score(\%) = 2 \times \frac{Precision \times Recall}{Precision + Recall} \times 100 \quad (6)$$

The use of precision, recall, and F1 score helps provide a more comprehensive evaluation of the model's performance, especially in cases where the dataset might have imbalanced classes. These metrics give insight into how well the model is performing in terms of correctly identifying the classes, while minimizing false positives and false negatives.

3. Results and Discussion

3.1. Spectral Data Interpretation

Figure 4 depicts the spectra obtained from the hyperspectral images acquired using a ground-based hyperspectral imaging system module for garlic crops cultivated in open fields. The blue line shows the average spectrum from untreated garlic crops, the green line from those grown with standard fertilization, and the red line from crops receiving double fertilization. The overall spectral pattern was confirmed to be similar to that reported in existing studies [38]. The sharp spectrum change observed in the range of 680~720 nm has been confirmed to be attributed to the related red edge reflection [39]. The difference in average spectrum between 550 nm and 750 nm is attributed to variations in chlorophyll absorption and red shift due to differences in fertilization. This spectrum characteristic indicates variations in carotenoid absorption (550 nm) and chlorophyll absorption (750 nm) [40]. However, with the given spectral data alone it is challenging to clearly discern such differences. In other wavelength regions, distinguishing spectral differences is difficult, and even in shadow graphs, overlapping regions complicate the discrimination of fertilization differences in garlic. Hence, achieving more precise results would necessitate additional data processing and analysis techniques.

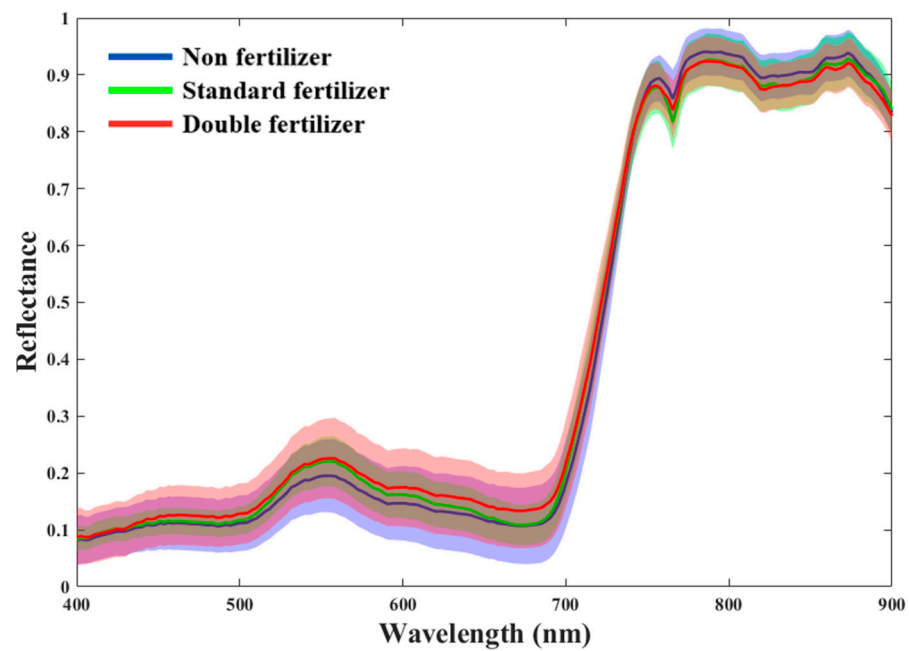


Figure 4. Garlic spectrum acquired by a ground-based hyperspectral imaging system module.

3.2. Analysis of the Impact of Fertilizer Application on Yield

In this study, a one-way analysis of variance (ANOVA) was conducted to evaluate the differences in yield among groups using three different fertilizer types. Table 4 provides a detailed comparison of the yield outcomes under the three different fertilizer treatments: non-treatment, standard, and double. Values marked by the same letter do not differ according to Tukey's honestly significant differences at the 5% confidence level in total fresh weight. There were significant differences among the groups, clearly indicating the impact of the three fertilizer types on garlic productivity. Similarly, differences in bulb fresh weight were also observed, with the double fertilizer treatment showing the most significant increase. However, there was no significant difference between the non-treat and standard fertilizer groups, which may be due to the measurements being taken in April, before the bulbs had fully developed. Additionally, the results obtained in May showed no significant difference between the standard and double fertilizer treatments, which is likely because the growth of the garlic bulbs stops once they reach a certain level of maturity. Therefore, even with the application of large amounts of fertilizer, the growth limit of garlic is fixed, indicating that it is economically important to apply the appropriate amount of fertilizer.

Table 4. Yield differences among fertilizers. Different letters (a, b, c) indicate statistically significant differences between groups. Values sharing the same letter are not significantly different from each other.

Month	Factor	Non-Treat	Standard	Double
April	Total fresh weight	107.60 ± 34.27 a	125.91 ± 41.42 b	144.21 ± 40.53 c
	Bulb fresh weight	18.27 ± 6.00 a	18.49 ± 6.07 a	21.34 ± 6.70 b
May	Total fresh weight	116.41 ± 35.63 a	144.92 ± 47.23 b	144.22 ± 48.09 b
	Bulb fresh weight	27.32 ± 7.84 a	30.20 ± 8.35 b	29.83 ± 8.31 b

3.3. Extraction of Optimal Wavelength

To enhance data processing efficiency the SFS, SPA, VIP, and iPLS methods were employed to identify the effective wavelength bands within the VIS/NIR spectrum of crops captured from ground-based hyperspectral imaging. The wavelength ranges of 525–725 nm

were found to be consistent with previous studies related to nitrogen stress [41]. Additionally, the wavelength at 548.4 nm is specifically associated with chlorophyll absorption, which is critical for assessing plant health and growth [42]. Using each method, 12 optimal wavelengths that effectively described the spectral data were identified. Selecting too few wavelengths can oversimplify the model, while selecting too many can increase computational complexity and introduce noise. Therefore, the decision to select 12 optimal wavelengths in this study reflects a careful balance aimed at capturing spectral information comprehensively, ensuring robustness across various selection methods, and prioritizing information to enhance model performance. Figure 5 is a frequency histogram showing how often each wavelength appears based on 12 optimal wavelengths adopted from four different methods. Table 5 lists the optimal wavelengths obtained using each method. Twelve different optimal wavelengths (405.9, 416.4, 463.9, 532.6, 548.4, 661.9, 688.3, 725.2, 741.0, 764.8, 846.6, and 886.2) were selected. Of the 12 wavelengths obtained through the four methods, we selected 12 optimal wavelengths, prioritizing wavelengths that significantly affect plant growth, chlorophyll content, nitrogen stress and frequency. Furthermore, to explore the feasibility of utilizing low-cost multispectral cameras instead of expensive hyperspectral cameras in agricultural environments, we considered the full width at half maximum (FWHM) with intervals of $\pm 3, 6, 9,$ and 12 nm around the selected wavelengths. This step ensures that our model can be adapted for practical, cost-effective applications in the field.

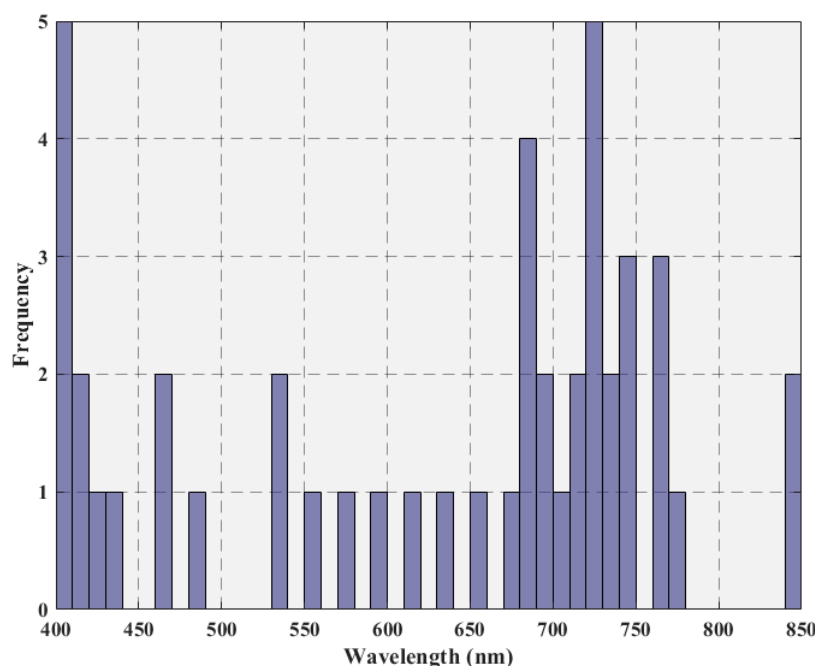


Figure 5. Frequency of selected wavelengths from SFS, SPA, VIP, iPLS.

Table 5. Optimal wavelength obtained from SFS, SPA, VIP, iPLS.

Methods	Numbers	Wavelengths (nm)
SFS	12	405.9, 427.0, 432.3, 463.9, 482.4, 532.6, 688.3, 741.0, 764.8, 770.1, 841.3, 846.6
SPA	12	400.6, 403.2, 405.9, 408.5, 411.2, 416.4, 463.9, 690.9, 725.2, 764.8, 886.2, 891.5
VIP	12	683.0, 685.6, 688.3, 690.9, 717.3, 719.9, 722.6, 725.2, 727.8, 730.5, 738.4, 741.0
iPLS	12	531.2, 552.3, 573.5, 594.6, 615.7, 636.8, 657.9, 679.0, 700.1, 721.2, 742.4, 763.5
Optimal	12	405.9, 416.4, 463.9, 532.6, 548.4, 661.9, 688.3, 725.2, 741.0, 764.8, 846.6, 886.2

3.4. Classification Model Results between Different Fertilization Groups

Table 6 and Figure 6 present the results of PLS-DA analyses conducted on the dataset acquired from garlic crops cultivated in open fields utilizing a ground-based hyperspectral imaging system module. Table 6 presents the detailed performance metrics for the partial

least squares discriminant analysis (PLS-DA) models used to classify fertilization levels in garlic crops. The included metrics are accuracy, precision, and F1 score, each offering different insights into the model's performance. Precision and F1 scores were used as indicators to ensure the model did not overfit. High precision ensures the model does not produce many false positives, while a high F1 score, reflecting the model's ability to generalize well without overfitting to the training data, indicates a good balance between precision and recall. When examining the results of the models based on the vegetation indices, a significant difference in accuracy is observed. This discrepancy may stem from the nonlinear characteristics inherent in the vegetation index data. Vegetation indices, which are commonly used to assess the growth status and health of plants, can exhibit complex, nonlinear relationships. These indices integrate various spectral bands to provide a comprehensive measure of vegetation properties, but their nonlinear nature poses challenges for certain types of models [43]. The PLS-DA model, although robust for linear relationships and useful for dimensionality reduction, may struggle to capture these intricate nonlinear patterns present in the vegetation index data. Traditional vegetation indices, such as the NDVI and PRI, have several limitations, particularly when capturing the complex spectral signatures associated with varying fertilizer treatments. Traditional indices often rely on a narrow range of spectral bands, which may oversimplify the complex interactions between light and plant tissues. This simplification can lead to a loss of valuable information critical for accurately assessing plant health and nutrient status. Furthermore, traditional indices may struggle to differentiate subtle variations in plant health and nutrient status, especially when the differences are not pronounced. This limitation is particularly relevant for detecting varying levels of fertilizer application, where the spectral differences may be minimal but significant. Hyperspectral imaging, on the other hand, captures a continuous spectrum of reflected light across a wide range of wavelengths, providing a much richer dataset. By capturing data across hundreds of narrow spectral bands, hyperspectral imaging can detect subtle changes in plant physiology that are not visible with traditional indices. This capability allows for a more precise assessment of plant health and nutrient status. The detailed spectral information enables better differentiation between different levels of fertilizer application, allowing for more accurate monitoring and management of crop nutrition.

Table 6. Results of fertilizer classification model.

	Class	Calibration			Validation		
		Accuracy (%)	Precision (%)	F1 Score (%)	Accuracy (%)	Precision (%)	F1 Score (%)
Vegetation indices	1–2	45.8	59.6	38.8	46.6	59.0	36.7
	2–3	48.4	58.1	50.4	47.8	59.3	51.7
	3–1	55.9	57.6	47.8	55.4	54.7	42.0
SFS	1–2	51.8	75.0	68.8	52.7	73.8	66.9
	2–3	59.7	85.4	79.3	59.3	84.6	78.2
	3–1	67.3	86.1	76.3	70.0	83.9	74.3
SPA	1–2	55.1	71.5	52.4	53.3	72.5	49.6
	2–3	65.3	74.5	72.9	64.7	74.5	73.2
	3–1	74.2	80.2	52.7	71.3	76.9	50.9
VIP	1–2	54.9	77.4	67.6	54.7	76.0	66.1
	2–3	65.5	80.2	76.8	65.3	79.0	75.0
	3–1	70.8	84.4	70.7	71.3	81.9	68.9
iPLS	1–2	51.6	77.8	74.0	52.0	76.4	71.9
	2–3	57.9	86.2	81.1	61.3	85.4	80.3
	3–1	67.7	93.0	83.1	66.0	91.7	81.9
Optimal wavelength	1–2	68.2	74.9	68.6	68.7	74.5	67.8
	2–3	76.7	84.5	79.1	73.7	84.9	79.2
	3–1	83.2	86.7	77.7	81.6	85.7	75.8
Optimal wavelength \pm 3 nm	1–2	67.7	75.6	70.3	65.5	76.3	72.0
	2–3	78.9	87.4	82.0	77.6	88.7	82.5
	3–1	86.2	90.2	80.7	83.6	91.3	82.6

Table 6. Cont.

	Class	Calibration			Validation		
		Accuracy (%)	Precision (%)	F1 Score (%)	Accuracy (%)	Precision (%)	F1 Score (%)
Optimal wavelength ± 6 nm	1–2	69.8	78.1	74.1	68.8	80.5	76.7
	2–3	80.9	88.5	83.2	79.0	88.6	83.1
	3–1	88.4	92.9	84.6	86.2	93.4	86.2
Optimal wavelength ± 9 nm	1–2	68.7	78.8	74.3	68.0	80.9	77.0
	2–3	81.7	87.6	82.7	79.1	87.7	82.9
	3–1	90.2	92.8	84.7	87.4	94.2	86.6
Optimal wavelength ± 12 nm	1–2	69.6	79.0	75.3	69.2	80.7	77.1
	2–3	82.6	89.9	84.8	79.5	90.3	84.7
	3–1	90.4	94.3	86.5	85.4	94.3	87.7
Full wavelength	1–2	80.7	81.8	78.3	82.0	82.2	79.5
	2–3	81.6	90.5	85.1	80.7	91.7	87.2
	3–1	93.8	95.0	88.1	90.7	96.3	89.9

The results of the classification models built using the 12 optimal wavelengths selected by SFS, SPA, VIP, and iPLS methods were compared. After evaluating the accuracy of the classification models using the wavelengths selected by each method individually, a new classification model was constructed by integrating the 12 optimal wavelengths derived from the four methods. The classification model using the integrated optimal wavelengths showed higher accuracy than the models using wavelengths selected by individual methods. This result confirmed the effectiveness of the integrated optimal wavelengths in enhancing classification performance. However, it was observed that the performance of the classification model based on these optimal wavelengths was lower than that of the model using the full wavelength range. Figure 7 illustrates the accuracy of the classification model when using optimal wavelengths across different ranges. To evaluate the impact of the full width at half maximum (FWHM), the optimal wavelengths were adjusted to five different ranges: optimal, ± 3 , ± 6 , ± 9 , and ± 12 nm. The impact of each range on the model's performance was evaluated. In this study, datasets composed of 12, 35, 56, 76, and 95 spectra were used. Initially, the model built with only the 12 optimal wavelengths showed low accuracy, likely due to insufficient diversity of wavelengths, which prevented the model from learning appropriate patterns. However, as the spectral range was expanded, an improvement in model performance was observed. When the optimal wavelengths were selected at intervals of ± 6 nm or more, accuracy levels comparable to those obtained using the full wavelength range were achieved. These results suggest that the improved stability of PLS-DA models can be attributed to the use of optimal wavelengths, providing enhanced robustness and reliability [44]. Consequently, selecting spectra based on optimal wavelengths and their respective ranges indicates that efficient data processing is achievable.

Using the full wavelength spectrum data, the PLS-DA model achieved classification accuracies of 82.0% for distinguishing between non-treatment and standard fertilization, 90.7% for distinguishing between non-treatment and double fertilization, and 80.7% for distinguishing between double fertilization and standard fertilization. These results effectively demonstrated the capability of hyperspectral imaging data in the VIS/NIR region to classify garlic crops based on different fertilization treatments. The high accuracy rates indicate that hyperspectral imaging, combined with advanced data analysis techniques like PLS-DA, can be a powerful tool for agricultural management. By accurately distinguishing between different levels of fertilization, this technology can help optimize fertilization practices, leading to better crop management and potentially higher yields.

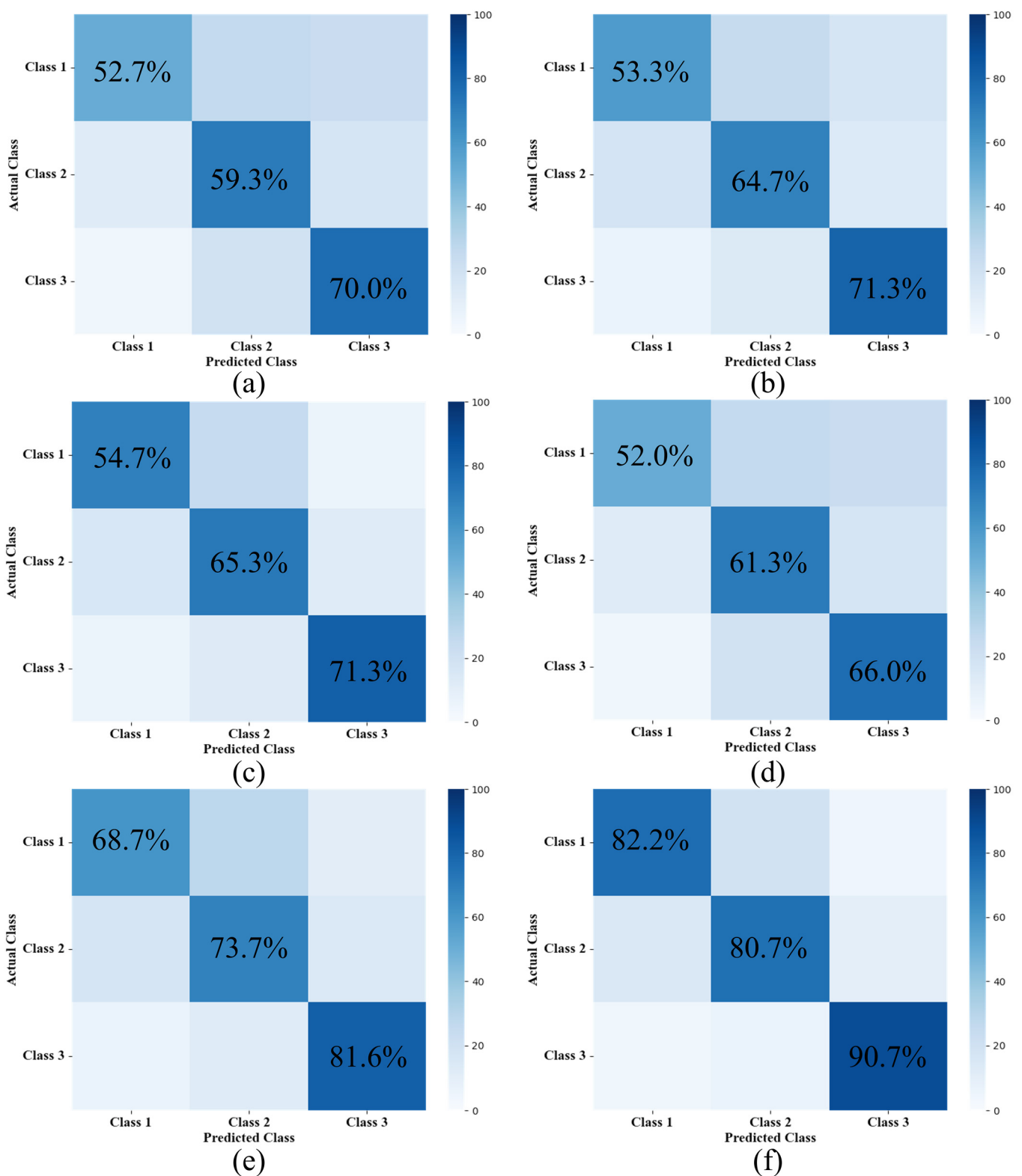


Figure 6. Confusion matrix for classification model based on fertilizer application at different wavelengths. (a) SFS; (b) SPA; (c) VIP; (d) iPLS; (e) optimal wavelength; (f) full wavelength.

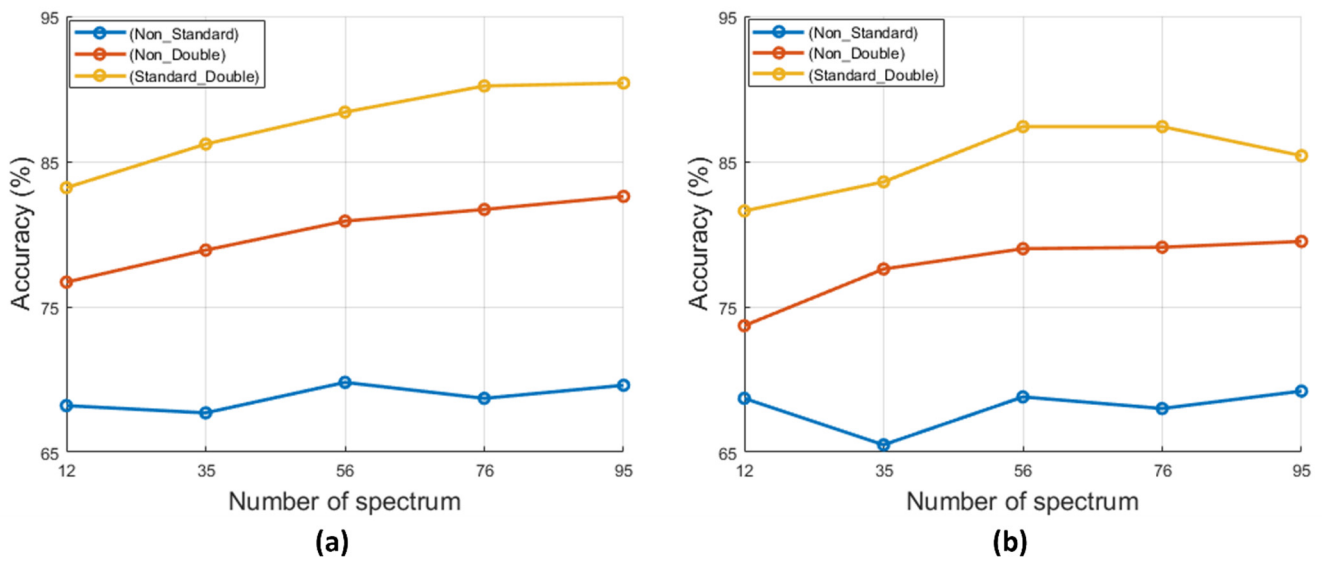


Figure 7. Classification model accuracy across different optimal wavelength ranges (± 0 , ± 3 , ± 6 , ± 9 , ± 12 nm). (a) Calibration; (b) validation.

3.5. Applying Classification Model Results to Different Fertilization Groups in Hyperspectral Images

Figure 8 presents NDVI images, images employing a classification model based on the full spectrum dataset, and images utilizing a classification model derived from the optimal spectrum dataset. The primary objective was to discern and analyze differences in fertilization treatments among these images. NDVI images, which rely on specific wavelengths of light to estimate and compare chlorophyll content and plant vitality, did not conclusively show differences in fertilization treatments within the wavelength range considered. This indicates a potential limitation of NDVI images in capturing subtle variations attributed to fertilization treatments. However, the application of machine learning-based classification models, utilizing both the full spectrum and optimal spectrum datasets, effectively accentuated differences among fertilization treatments. These classification images amalgamated diverse optical and statistical techniques to discern more sensitive disparities, facilitating a more accurate understanding of plant growth and response to fertilization treatments. Consequently, the garlic crop model images utilized in this study can be effectively utilized to extract growth-related information concerning garlic crop fertilization treatments.

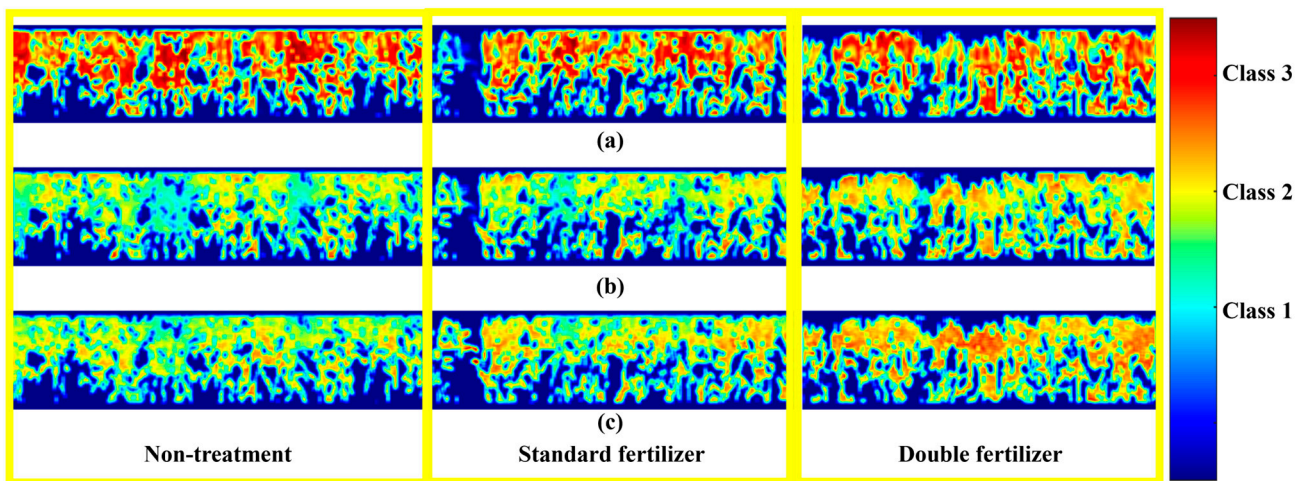


Figure 8. Image of garlic field. (a) NDVI, (b) optimal-wavelength applied PLS-DA, (c) full-wavelength applied PLS-DA.

3.6. Discussion

This study developed and validated a model for classifying fertilization levels in garlic crops grown in open fields using VIS/NIR hyperspectral images. The results demonstrated that differences in fertilization levels which were not discernible using conventional vegetation indices could be successfully identified through hyperspectral imaging. The high spectral resolution of hyperspectral images effectively detects subtle physiological changes in crops. Previous studies have demonstrated that traditional vegetation indices, such as NDVI, have limitations in capturing the complex spectral features associated with varying fertilizer treatments. The NDVI can be influenced by factors such as soil background, atmospheric conditions, and canopy structure, leading to inaccuracies in assessing plant health and nutrient status [23]. In contrast, hyperspectral imaging provides a continuous spectrum of reflected light across a wide range of wavelengths, allowing for a more precise assessment of plant health and nutrient status. The results of this study using hyperspectral imaging highlight its superiority in detecting subtle differences in fertilization levels that were not discernible using conventional vegetation indices. This study distinguishes itself by focusing on garlic crops and addressing various fertilization levels. Despite the high cost and complexity of hyperspectral imaging systems, this study suggests that multispectral imaging could serve as a more cost-effective alternative. Habibullah, Mohebian [45] has proposed methods for monitoring physiological changes in crops using low-cost multispectral imaging, and this study extends that approach to differentiate fertilization levels, indicating that multispectral imaging can be a practical alternative. Notably, the PLS model using the optimal wavelength ranges achieved a high accuracy of 85.4% in classifying non-fertilized and double-fertilized conditions. These results highlight the effectiveness of using optimal wavelength ranges in multispectral imaging to precisely classify fertilization levels in garlic crops, expanding its applicability in agriculture. The selection of the 12 optimal wavelengths, based on their physiological relevance to garlic growth and fertilizer response, provides a crucial foundation for developing targeted multispectral cameras. By focusing on these specific wavelengths, we can design multispectral cameras that are not only cost-effective but also tailored to capture critical information about crop health and nutrient status. This targeted approach can significantly improve the efficiency and accuracy of agricultural monitoring systems. Furthermore, the study presents the potential of developing low-cost multispectral imaging systems, making advanced imaging technologies accessible to a broader range of farmers. By monitoring physiological changes in crops and optimizing fertilizer use, this technology can significantly enhance the sustainability and efficiency of agricultural practices. The ability to use specific wavelengths to detect subtle changes in plant health allows for more precise interventions, reducing the need for excessive fertilizer application and minimizing environmental impact. In addition, this study's hyperspectral/multispectral approach can significantly enhance the accuracy and timeliness of fertilizer management in garlic cultivation. One of the main challenges in current practices is over-fertilization, which can lead to nutrient leaching, soil degradation, and increased production costs. By using hyperspectral imaging to monitor the physiological changes in garlic crops, the early signs of over-fertilization can be detected, allowing timely adjustments in fertilizer application. This precise monitoring helps prevent excessive fertilizer use, promotes sustainable agricultural practices, and reduces environmental impact. Moreover, the specific wavelengths identified in our study can be used to develop targeted multispectral cameras. These cameras can be integrated into existing farm management systems, providing farmers with accessible and cost-effective tools for precision agriculture. By focusing on the most useful spectral bands, multispectral imaging systems can be more affordable and easier to deploy than full hyperspectral systems, while still offering high accuracy in assessing crop health and fertilization levels. This technology can enable real-time monitoring and early detection of plant health issues, facilitating more proactive and efficient farming practices. Developing portable and affordable multispectral cameras based on the identified optimal wavelengths can revolutionize precision agriculture, making it more accessible and effective for smallholder farmers.

3.7. Limitations

This study focused on garlic crops cultivated during the spring season, acknowledging the significant impact of seasonal variations on crop growth and physiological responses. It is essential to evaluate whether data and models derived from spring garlic can be effectively applied to garlic cultivation in other seasons. This necessitates additional data collection and analysis across different seasons. Furthermore, factors such as soil type, climate conditions, and garlic variety can significantly influence model performance. The soil type affects garlics growth and the spectral characteristics, posing challenges for developing a single model that accurately classifies fertilization levels across diverse soil conditions. Future research could explore developing models specific to certain soil types or more generalized models incorporating data from various soil conditions. Climate conditions also play a crucial role, as seasonal changes and extreme weather events can affect spectral data and thereby impact model performance. Future studies should consider collecting data from different climatic conditions to develop robust models that perform consistently across various environmental scenarios. Additionally, different garlic varieties may respond differently to fertilization, affecting spectral data variability and model generalizability. While this study focused on a specific garlic variety, future research should expand to include multiple varieties to better understand their impact on model performance.

To enhance the model's generalizability and robustness, it is essential to expand the scope of data collection and analysis. This includes gathering spectral data from different geographical regions and various garlic varieties. By considering diverse environmental and biological conditions, the model can be refined to provide more accurate and reliable predictions across a broader range of scenarios. Addressing these factors is crucial for developing adaptive models that can accommodate variations in soil types, climate conditions, and garlic varieties, ultimately improving the model's applicability and effectiveness in real-world agricultural practices.

In conclusion, while this study provides a foundation for classifying fertilization levels in garlic crops using hyperspectral imaging, addressing these factors is crucial for enhancing the model's robustness and generalizability. Future research efforts should focus on collecting and analyzing spectral data across diverse soil types and climate conditions, investigating the impact of different garlic varieties, and developing adaptive models to accommodate these variations effectively.

4. Conclusions

In this study, we aimed to develop a model for classifying fertilization levels in garlic crops grown in open fields using VIS/NIR hyperspectral images. The conclusions are as follows: (1) Differences in the fertilization levels of garlic crops, which were not discernible using conventional vegetation indices, were successfully identified using hyperspectral images. The results obtained from modeling based on hyperspectral image data in the VIS/NIR range, utilizing six traditional vegetation indices (NDVI, PRI, RDVI, GNDVI, CI, and TCARI), revealed differences in fertilization levels among garlic crops, although these traditional vegetation indices have shown limited effectiveness. (2) Hyperspectral imaging systems capture data across hundreds of narrow spectral bands, providing high spectral resolution. This enables detection of subtle physiological and health changes in plants that are not observable with conventional or multispectral imaging systems. However, the cost of hyperspectral imaging equipment is significantly higher due to the complexity and precision required by the sensors. In contrast, multispectral imaging captures data across fewer, broader spectral bands. While the spectral resolution is lower, multispectral sensors are less complex, more affordable, and easily integrable into existing agricultural machinery and practices. By carefully selecting relevant spectral bands and integrating multispectral imaging into farm management practices, farmers can enhance fertilizer management and improve crop productivity. In our study, the PLS model using the full wavelength range achieved an accuracy of 90.7% in distinguishing between non-fertilized

and double-fertilized conditions. In contrast, the combined accuracy using the optimal 12 wavelengths selected from SFS, VIP, SPA, and iPLS was 81.6% for these conditions. However, we observed that expanding the spectral range while considering FWHM improves the accuracy of wavelength selection. This suggests the potential to develop a system capable of distinguishing fertilizer levels in crops using low-cost multispectral images instead of expensive hyperspectral images. (3) Our research shows that precise classification of fertilizer application using hyperspectral imaging and machine learning techniques can potentially lead to better-informed decisions regarding fertilizer use. This can result in improved growth conditions and ultimately higher yields. The ability to differentiate fertilizer effects accurately will enable more targeted interventions, thus contributing to increased farm productivity in the long run. We anticipate that the implementation of our findings will provide valuable insights for future studies and practical applications in agriculture, promoting sustainable and efficient farming practices. By leveraging the high-resolution data from hyperspectral imaging, researchers can develop more precise models to optimize fertilization strategies, enhancing crop health and yield predictions. This can lead to tailored fertilizer use, reducing environmental impacts. Moreover, adopting hyperspectral imaging technology can enable real-time monitoring and early detection of crop health issues, fostering proactive and efficient farming practices. This technology's integration into farm management systems can significantly improve decision-making processes, leading to better crop management and resource use. Additionally, our findings can inspire the development of cost-effective multispectral imaging systems, making advanced imaging technologies more accessible to a broader range of farmers. We anticipate that the implementation of our findings will provide valuable insights for future studies and practical applications in agriculture, promoting sustainable and efficient farming practices.

Author Contributions: Conceptualization, H.L. and B.-K.C.; methodology, H.C.; collected the data, H.C.; software, H.C.; validation, H.C.; formal analysis, H.C.; investigation, H.C.; resources, S.W.; data curation, H.C.; writing—original draft preparation, H.C.; writing—review and editing, H.L.; visualization, H.C.; supervision, H.L. and B.-K.C.; project administration, H.L. All authors have read and agreed to the published version of the manuscript.

Funding: This work was supported by the Korea Institute of Planning and Evaluation for Technology in Food, Agriculture, and Forestry (IPET) through the Open Field Smart Agriculture Technology Short-term Advancement Program, funded by the Ministry of Agriculture, Food, and Rural Affairs (MAFRA) (grant number: 322032-3).

Institutional Review Board Statement: Not applicable.

Data Availability Statement: Data are contained within the article.

Conflicts of Interest: The authors declare no conflicts of interest.

References

- Omar, S.H.; Hasan, A.; Hunjul, N.; Ali, J.; Aqil, M. Historical, chemical and cardiovascular perspectives on garlic: A review. *Pharmacogn. Rev.* **2007**, *1*, 80–87.
- Papu, S.; Jaivir, S.; Sweta, S.; Singh, B. Medicinal values of garlic (*Allium sativum* L.) in human life: An overview. *Greener J. Agric. Sci.* **2014**, *4*, 265–280.
- Bisht, N.; Chauhan, P.S. Excessive and disproportionate use of chemicals cause soil contamination and nutritional stress. In *Soil Contamination-Threats and Sustainable Solutions*; IntechOpen: London, UK, 2020; pp. 1–10.
- Lee, D.-H.; Shin, H.-S.; Park, J.-H. Developing a p-NDVI map for highland kimchi cabbage using spectral information from UAVs and a field spectral radiometer. *Agronomy* **2020**, *10*, 1798. [[CrossRef](#)]
- Lu, B.; Dao, P.D.; Liu, J.; He, Y.; Shang, J. Recent advances of hyperspectral imaging technology and applications in agriculture. *Remote Sens.* **2020**, *12*, 2659. [[CrossRef](#)]
- Kiani, S.; van Ruth, S.M.; Minaei, S.; Ghasemi-Varnamkhasti, M. Hyperspectral imaging, a non-destructive technique in medicinal and aromatic plant products industry: Current status and potential future applications. *Comput. Electron. Agric.* **2018**, *152*, 9–18. [[CrossRef](#)]
- Nalepa, J. Recent advances in multi-and hyperspectral image analysis. *Sensors* **2021**, *21*, 6002. [[CrossRef](#)] [[PubMed](#)]
- Ravikanth, L.; Jayas, D.S.; White, N.D.; Fields, P.G.; Sun, D.-W. Extraction of spectral information from hyperspectral data and application of hyperspectral imaging for food and agricultural products. *Food Bioprocess Technol.* **2017**, *10*, 1–33. [[CrossRef](#)]

9. Wang, C.; Liu, B.; Liu, L.; Zhu, Y.; Hou, J.; Liu, P.; Li, X. A review of deep learning used in the hyperspectral image analysis for agriculture. *Artif. Intell. Rev.* **2021**, *54*, 5205–5253. [[CrossRef](#)]
10. Tao, H.; Feng, H.; Xu, L.; Miao, M.; Yang, G.; Yang, X.; Fan, L. Estimation of the yield and plant height of winter wheat using UAV-based hyperspectral images. *Sensors* **2020**, *20*, 1231. [[CrossRef](#)]
11. Baek, I.; Lee, H.; Cho, B.-k.; Mo, C.; Chan, D.E.; Kim, M.S. Shortwave infrared hyperspectral imaging system coupled with multivariable method for TVB-N measurement in pork. *Food Control* **2021**, *124*, 107854. [[CrossRef](#)]
12. Geipel, J.; Bakken, A.K.; Jørgensen, M.; Korsæth, A. Forage yield and quality estimation by means of UAV and hyperspectral imaging. *Precis. Agric.* **2021**, *22*, 1437–1463. [[CrossRef](#)]
13. Gui, J.; Fei, J.; Wu, Z.; Fu, X.; Diakite, A. Grading method of soybean mosaic disease based on hyperspectral imaging technology. *Inf. Process. Agric.* **2021**, *8*, 380–385. [[CrossRef](#)]
14. Sabzi, S.; Pourdarbani, R.; Rohban, M.H.; Fuentes-Penna, A.; Hernández-Hernández, J.L.; Hernández-Hernández, M. Classification of cucumber leaves based on nitrogen content using the hyperspectral imaging technique and majority voting. *Plants* **2021**, *10*, 898. [[CrossRef](#)] [[PubMed](#)]
15. Chu, X.; Miao, P.; Zhang, K.; Wei, H.; Fu, H.; Liu, H.; Jiang, H.; Ma, Z. Green Banana maturity classification and quality evaluation using hyperspectral imaging. *Agriculture* **2022**, *12*, 530. [[CrossRef](#)]
16. Kim, G.; Lee, H.; Baek, I.; Cho, B.-K.; Kim, M.S. Quantitative detection of benzoyl peroxide in wheat flour using line-scan short-wave infrared hyperspectral imaging. *Sens. Actuators B Chem.* **2022**, *352*, 130997. [[CrossRef](#)]
17. Adão, T.; Hruška, J.; Pádua, L.; Bessa, J.; Peres, E.; Morais, R.; Sousa, J.J. Hyperspectral imaging: A review on UAV-based sensors, data processing and applications for agriculture and forestry. *Remote Sens.* **2017**, *9*, 1110. [[CrossRef](#)]
18. Quemada, M.; Gabriel, J.L.; Zarco-Tejada, P. Airborne hyperspectral images and ground-level optical sensors as assessment tools for maize nitrogen fertilization. *Remote Sens.* **2014**, *6*, 2940–2962. [[CrossRef](#)]
19. Ra, S. *Garlic Cultivation (Agricultural Technical Guide 117)*; Rural Development Administration: Jeonju, Republic of Korea, 2017.
20. Garbulska, M.F.; Peñuelas, J.; Gamon, J.; Inoue, Y.; Filella, I. The photochemical reflectance index (PRI) and the remote sensing of leaf, canopy and ecosystem radiation use efficiencies: A review and meta-analysis. *Remote Sens. Environ.* **2011**, *115*, 281–297. [[CrossRef](#)]
21. Radočaj, D.; Šiljeg, A.; Marinović, R.; Jurišić, M. State of major vegetation indices in precision agriculture studies indexed in web of science: A review. *Agriculture* **2023**, *13*, 707. [[CrossRef](#)]
22. Ihuoma, S.O.; Madramootoo, C.A. Recent advances in crop water stress detection. *Comput. Electron. Agric.* **2017**, *141*, 267–275. [[CrossRef](#)]
23. Zeng, Y.; Hao, D.; Huete, A.; Dechant, B.; Berry, J.; Chen, J.M.; Joiner, J.; Frankenberg, C.; Bond-Lamberty, B.; Ryu, Y. Optical vegetation indices for monitoring terrestrial ecosystems globally. *Nat. Rev. Earth Environ.* **2022**, *3*, 477–493. [[CrossRef](#)]
24. Gago, J.; Douthe, C.; Coopman, R.E.; Gallego, P.P.; Ribas-Carbo, M.; Flexas, J.; Escalona, J.; Medrano, H. UAVs challenge to assess water stress for sustainable agriculture. *Agric. Water Manag.* **2015**, *153*, 9–19. [[CrossRef](#)]
25. Rouse, J.W.; Haas, R.H.; Schell, J.A.; Deering, D.W. Monitoring vegetation systems in the Great Plains with ERTS. *NASA Spec. Publ.* **1974**, *351*, 309.
26. Gitelson, A.A.; Kaufman, Y.J.; Merzlyak, M.N. Use of a green channel in remote sensing of global vegetation from EOS-MODIS. *Remote Sens. Environ.* **1996**, *58*, 289–298. [[CrossRef](#)]
27. Roujean, J.-L.; Breon, F.-M. Estimating PAR absorbed by vegetation from bidirectional reflectance measurements. *Remote Sens. Environ.* **1995**, *51*, 375–384. [[CrossRef](#)]
28. Gitelson, A.A.; Gritz, Y.; Merzlyak, M.N. Relationships between leaf chlorophyll content and spectral reflectance and algorithms for non-destructive chlorophyll assessment in higher plant leaves. *J. Plant Physiol.* **2003**, *160*, 271–282. [[CrossRef](#)] [[PubMed](#)]
29. Eitel, J.; Long, D.; Gessler, P.; Hunt Jr, E.; Brown, D. Sensitivity of ground-based remote sensing estimates of wheat chlorophyll content to variation in soil reflectance. *Soil Sci. Soc. Am. J.* **2009**, *73*, 1715–1723. [[CrossRef](#)]
30. Tunny, S.S.; Amanah, H.Z.; Faqeerzada, M.A.; Wakholi, C.; Kim, M.S.; Baek, I.; Cho, B.-K. Multispectral wavebands selection for the detection of potential foreign materials in fresh-cut vegetables. *Sensors* **2022**, *22*, 1775. [[CrossRef](#)]
31. Aha, D.W.; Bankert, R.L. A comparative evaluation of sequential feature selection algorithms. In Proceedings of the Pre-proceedings of the Fifth International Workshop on Artificial Intelligence and Statistics, Fort Lauderdale, FL, USA, 4–7 January 1995; pp. 1–7.
32. Soares, S.F.C.; Gomes, A.A.; Araujo, M.C.U.; Galvão Filho, A.R.; Galvão, R.K.H. The successive projections algorithm. *TrAC Trends Anal. Chem.* **2013**, *42*, 84–98. [[CrossRef](#)]
33. Liu, D.; Sun, D.-W.; Zeng, X.-A. Recent advances in wavelength selection techniques for hyperspectral image processing in the food industry. *Food Bioprocess Technol.* **2014**, *7*, 307–323. [[CrossRef](#)]
34. Fu, J.; Yu, H.-D.; Chen, Z.; Yun, Y.-H. A review on hybrid strategy-based wavelength selection methods in analysis of near-infrared spectral data. *Infrared Phys. Technol.* **2022**, *125*, 104231. [[CrossRef](#)]
35. Rinnan, Å.; Van Den Berg, F.; Engelsen, S.B. Review of the most common pre-processing techniques for near-infrared spectra. *TrAC Trends Anal. Chem.* **2009**, *28*, 1201–1222. [[CrossRef](#)]
36. Chevallier, S.; Bertrand, D.; Kohler, A.; Courcoux, P. Application of PLS-DA in multivariate image analysis. *J. Chemom. A J. Chemom. Soc.* **2006**, *20*, 221–229. [[CrossRef](#)]
37. Geladi, P.; Kowalski, B.R. Partial least-squares regression: A tutorial. *Anal. Chim. Acta* **1986**, *185*, 1–17. [[CrossRef](#)]

38. Rodrigues, M.; Nanni, M.R.; Cezar, E.; dos Santos, G.L.A.A.; Reis, A.S.; de Oliveira, K.M.; de Oliveira, R.B. Vis–NIR spectroscopy: From leaf dry mass production estimate to the prediction of macro-and micronutrients in soybean crops. *J. Appl. Remote Sens.* **2020**, *14*, 044505. [[CrossRef](#)]
39. Horler, D.; Dockray, M.; Barber, J.; Barringer, A. Red edge measurements for remotely sensing plant chlorophyll content. *Adv. Space Res.* **1983**, *3*, 273–277. [[CrossRef](#)]
40. Van Wittenberghe, S.; Alonso, L.; Malenovský, Z.; Moreno, J. In vivo photoprotection mechanisms observed from leaf spectral absorbance changes showing VIS–NIR slow-induced conformational pigment bed changes. *Photosynth. Res.* **2019**, *142*, 283–305. [[CrossRef](#)]
41. Ye, X.; Abe, S.; Zhang, S. Estimation and mapping of nitrogen content in apple trees at leaf and canopy levels using hyperspectral imaging. *Precis. Agric.* **2020**, *21*, 198–225. [[CrossRef](#)]
42. Wang, Y.; Hu, X.; Jin, G.; Hou, Z.; Ning, J.; Zhang, Z. Rapid prediction of chlorophylls and carotenoids content in tea leaves under different levels of nitrogen application based on hyperspectral imaging. *J. Sci. Food Agric.* **2019**, *99*, 1997–2004. [[CrossRef](#)]
43. Kok, Z.H.; Shariff, A.R.M.; Alfatni, M.S.M.; Khairunniza-Bejo, S. Support vector machine in precision agriculture: A review. *Comput. Electron. Agric.* **2021**, *191*, 106546. [[CrossRef](#)]
44. Wan, G.; Liu, G.; He, J.; Luo, R.; Cheng, L.; Ma, C. Feature wavelength selection and model development for rapid determination of myoglobin content in nitrite-cured mutton using hyperspectral imaging. *J. Food Eng.* **2020**, *287*, 110090. [[CrossRef](#)]
45. Habibullah, M.; Mohebian, M.R.; Soolanayakanahally, R.; Bahar, A.N.; Vail, S.; Wahid, K.A.; Dinh, A. Low-cost multispectral sensor array for determining leaf nitrogen status. *Nitrogen* **2020**, *1*, 67–80. [[CrossRef](#)]

Disclaimer/Publisher’s Note: The statements, opinions and data contained in all publications are solely those of the individual author(s) and contributor(s) and not of MDPI and/or the editor(s). MDPI and/or the editor(s) disclaim responsibility for any injury to people or property resulting from any ideas, methods, instructions or products referred to in the content.